PAPER

Energy selectivity in electron absorptive heating methods: does the angular momentum trap matter? An experimental investigation

To cite this article: Chi-Shung Yip et al 2022 Plasma Sources Sci. Technol. 31 084003

View the article online for updates and enhancements.

You may also like

- Feedback-controlled heat transport in quantum devices: theory and solid-state experimental proposal
 Michele Campisi, Jukka Pekola and Rosario Fazio
- Quantum consensus dynamics by entangling Maxwell demon Sungguen Ryu, Rosa López and Raúl Toral
- <u>Stochastic thermodynamics for "Maxwell demon" feedbacks</u>
 Massimiliano Esposito and Gernot Schaller



Energy selectivity in electron absorptive heating methods: does the angular momentum trap matter? An experimental investigation

Chi-Shung Yip^{1,*}, Chenyao Jin^{1,2}, Wei Zhang^{1,*}, Di Jiang¹, Young-Chul Ghim³ and Greg Severn⁴

- ¹ Institute of Plasma Physics, Chinese Academy of Sciences, Hefei 230031, People's Republic of China
- ² University of Science and Technology of China, Hefei, Anhui 230026, People's Republic of China
- ³ Department of Nuclear and Quantum Engineering, Korea Advanced Institute of Science and Technology, Daejeon 34141, Republic of Korea
- ⁴ Department of Physics & Biophysics, University of San Diego, San Diego, CA 92110, United States of America

E-mail: csyip@ipp.ac.cn and zhangwei@ipp.ac.cn

Received 29 March 2022, revised 13 July 2022 Accepted for publication 25 July 2022 Published 11 August 2022



Abstract

Comparison between the Maxwell demon and a planar electrode has been revisited with an in-depth analysis of whether the angular momentum trap of the Maxwell demon indeed provides better energy selectivity than a small planar electrode that absorbs electrons indiscriminately. The evolutions of the EEDF under the influence of these heating techniques is directly analyzed, as well as the resultant plasma parameters. Experimental results show that the Maxwell demon indeed provides better energy selectivity as shown by its better retention of hot electrons than an indiscriminative absorption surface, which in turn results in smaller disturbance to the plasma potential a smaller reduction of the plasma density in the heating process. Experimental result also shows no electron heating when the demon is replaced by an ion-sheath forming large electrode, this is consistent with Mackenzie's original results (MacKenzie *et al* 1971 *App. Phys. Lett.* **18** 529). While it is possible to obtain the exact same plasma parameters replacing the Maxwell demon with a suitably sized planar plate and additional plasma parameters control, for experiments sensitive to the exact processes from which plasma parameters are formed, one should not overlook the physical differences of these heating methods.

Keywords: EEDFs, electron heating, Maxwell's demon, electron sheath

(Some figures may appear in colour only in the online journal)

1. Introduction

Control of the electron energy distribution function (EEDF) has been a very important aspect in the study of plasma physics: sheath and plasma potential formation depends on the effective electron temperature, features of the EEDF can affect

* Authors to whom any correspondence should be addressed.

plasma instability formation, and the availability of electrons at different energies controls chemical processes in plasma processing. As such, EEDF tailoring techniques that enables independent adjustment of the electron temperature $T_{\rm e}$ without changing plasma source operation, neutral pressure, or gas composition are very desirable tools in these experimental studies, even if their uses are limited to basic plasma research. One such simple way to control $T_{\rm e}$, as proposed by Mackenzie

[1], is to immerse a grid of very thin wires into a plasma and bias it positively, so that the grid serves as an angular momentum trap to the electrons and tailors the EEDF via selectively removing cold electrons from a plasma. This device is now known as Mackenzie's Maxwell demon. On the other hand, Yip et al [2, 3] and Baalrud et al [4-7] found that a very similar effect can be achieved by simply putting a solid plate of proper size into the plasma and biasing it positively, as a small electrode can form an electron sheath and serves as an indiscriminative loss area to electrons. The indiscriminative loss effect increases low energy electron loss, raises the plasma potential and removes the energy selectivity of the sheath of the device wall, causing plasma to be heated. If angular momentum trap effect of Mackenzie's Maxwell demon indeed exists, it could be very different from an indiscriminative loss area, i.e. a small solid electrode, because it both selectively removes cold electrons and retain more energetic ones, as opposed to absorbing both kinds of electrons in an indiscriminative manner. Due to this difference in energy selectivity, the relationship between an angular trap's heating effect can be very different than its effect on the bulk plasma potential, as we will show as we compare both effects as they are related to thin wire grids, i.e. MacKenzie's Maxwell demon, and solid plates. Therefore, other than simply changing an effective $T_{\rm e}$, the two different methods are supposed to tailor the EEDF in different ways, provided that their underlying principles are indeed what was previously found to be. Thus, this work presents direct comparison of the effects of the two different EEDF tailoring methods to the form of the EEDF other than just the effective $T_{\rm e}$, to examine the different physical processes between these heating methods.

In section 2, the analytic models of how the two different heating methods changes the EEDF are presented. Section 3 provides a description of the experimental setup. Experimental results and their associated discussions are given in section 4. The conclusions of this work is presented in section 5.

2. Electron heating via absorption techniques

In this section we will briefly review the analytical models of the heating mechanisms for the two different electron absorption heating methods, namely using a small solid plate as an indiscriminative electron sink, which is associated with the energy selectivity of the sheath, and the Maxwell demon grid, which is associated with the energy selectivity of an angular momentum trap.

2.1. Energy selectivity of the sheath near a solid surface

Sheath loss cone as a EEDF tailoring effect has long been investigated for prediction of EEDF evolution in low temperature plasma devices [8–11]. Here we crudely revisit this effect to compare qualitatively with the EEDF tailoring effect of the angular momentum trap.

When electrons of a bound plasma incident onto the device wall, the sheath reflects away all electrons with kinetic energy $E_{\rm e}$ below the sheath potential barrier $eV_{\rm sh}$, confining the low energy electrons. For electrons with $E_{\rm e} > eV_{\rm sh}$, only electrons

within the loss cone, i.e. $E_{\rm e,z}=E_{\rm e}\cos^2(\varphi)>eV_{\rm sh}$ overcomes the sheath potential and becomes lost. Consider proportion of the solid angle formed by φ in 3D space $2\pi(1-\cos(\varphi))$ compared with the half-sphere total incident angle 2π . With this one can consider a very crude approximation of the energy differential loss flux to the wall ${\rm d}\Gamma_{\rm e}(E_{\rm e})$ of an isotropic Maxwellian EEDF $f_{\rm e}(E_{\rm e})$ to obtain

$$d\Gamma_{\text{wall}}(E_{\text{e}}) = v_{\text{e,z}}(E_{\text{e}}) f_{\text{e}}(E_{\text{e}}) n_{\text{e}} A_{\text{wall}} \Omega_{\text{loss}}(E_{\text{e}}) dE_{\text{e}}, \qquad (1)$$

where $\Omega_{\rm loss}$ is the normalized solid angle $(1-\cos(\varphi))=1-(eV_{\rm sh}/E_{\rm e})^{1/2}$. Note that the loss flux to the wall $\Gamma_{\rm wall}=\int v_{\rm e}(E_{\rm e})f_{\rm e}(E_{\rm e})\Omega_{\rm loss}\,{\rm d}E_{\rm e}$ is the integral of the energy differential loss flux over all $E_{\rm e}$. A sample of $V_{\rm sh}$ normalized solid angle with various $eV_{\rm sh}/T_{\rm e}$ and the associated normalized differential loss flux $({\rm d}\Gamma_{\rm wall}/{\rm d}(E_{\rm e}/T_{\rm e}))/(v_{\rm e,th}n_{\rm e}A_{\rm wall})=v_{\rm e}(E_{\rm e})/v_{\rm e,th}T_{\rm e}f_{\rm e}(E_{\rm e}/T_{\rm e})\Omega_{\rm loss}$ where $v_{\rm e,th}=(2T_{\rm e}/m_{\rm e})^{1/2}$ is the electron most probable speed in a Maxwellian EEDF is shown in figures 1(a) and (b).

Generally, when the device wall is grounded and conductive, and without other confinement associated effects, $V_{\rm sh}$ is also the plasma potential $V_{\rm p}$, and in low temperature plasmas $V_{\rm sh} \sim V_{\rm p}$ is approximately $3-5T_{\rm e}/e$ as a result of ion–electron loss balance [7, 12], and could be limited to above the ionization energy $E_{\rm iz}$ to confine ionizing electrons [10]. However, plasmas with multi-dipole confinement, as with the one employed in this work, can effectively reduce electron loss area and cause $V_{\rm p}$ to be reduced.

Without considering the formation of an anode spot or a fireball [4, 6, 7, 13–15], a positively biased electrode is inserted into the bulk plasma either forms an electron sheath, a virtual cathode, or an ion sheath causing the plasma potential to follow the electrode potential [4–7]. Generally, an electron sheath can only form when the electrode is sufficiently small such that $A_{\rm electrode} < 2.3 A_{\rm wall} (m_e/m_i)^{1/2}$ [4–7], where $A_{\rm electrode}$ and $A_{\rm wall}$ are the area of the electrode and the device wall respectively. When an electron sheath forms, the electrode becomes an indiscriminative loss area to electrons, and therefore facilitates additional loss of cold electrons. The energy differential loss flux to the electrode assuming a Maxwellian EEDF is simply

$$d\Gamma_{\text{electrode}}(E_{\text{e}}) = A_{\text{electrode}} n_{\text{e}} v_{\text{e}}(E_{\text{e}}) f_{\text{e}}(E_{\text{e}}) dE_{\text{e}}, \tag{2}$$

where $A_{\rm electrode}$ is the electron absorption area of the unselective loss surface. One should note that as shown in equation (2), as an energy unselective loss flux, $d\Gamma_{\rm electrode}$ is only energy dependent from the incident electron flux $n_{\rm e}v_{\rm e}(E_{\rm e})f_{\rm e}(E_{\rm e})$, and the amplitude of the $d\Gamma_{\rm electrode}$ depends only on electrode size. Thus $d\Gamma_{\rm electrode}$ is, on principle, independent on the bias voltage applied on the electrode. However, experimentally an increasing bias voltage thickens the sheath near an electrode and cause its effective area to expand, increasing $A_{\rm electrode}$, therefore allowing it to heat the plasma as a larger electrode and further raise $T_{\rm e}$. This effect will be discussed in the later sections

A normalized $(d\Gamma_{electrode}/d(E_e/T_e))/(v_{e,th}n_eA_{electrode}) = (v_e(E_e)/v_{e,th})T_ef(E_e/T_e)$ is graphed assuming a Maxwellian EEDF in figure 1(c). As shown in the figure, the differential

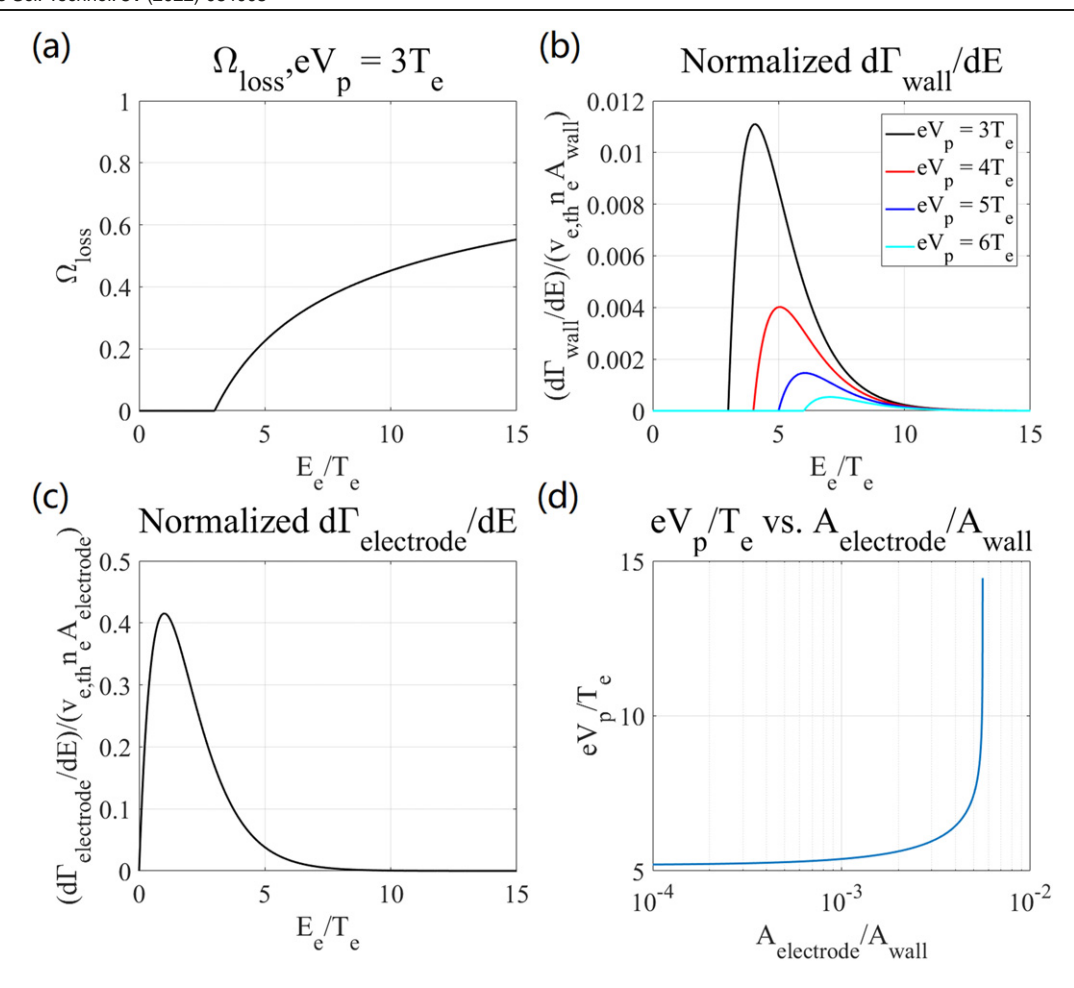


Figure 1. (a) The normalized solid angle of the loss cone vs total kinetic energy of the incident electron. (b) The differential loss flux $(d\Gamma_{\text{wall}}/dE)/(v_{\text{e,th}}n_{\text{e}}A_{\text{wall}})$ vs $E_{\text{e}}/T_{\text{e}}$ at various $eV_{\text{sh}}/T_{\text{e}}$. (c) The differential loss flux $(d\Gamma_{\text{electrode}}/dE)/(v_{\text{e,th}}n_{\text{e}}A_{\text{wall}})$ of electrons toward an energy unselective loss surface vs normalized electron energy $E_{\text{e}}/T_{\text{e}}$. (d) The evolution of the global plasma potential $eV_{\text{p}}/T_{\text{e}}$ under the influence of an additional electron absorbing electrode at various area ratio $A_{\text{electrode}}/A_{\text{wall}}$. The calculation assumes an argon plasma with $(m_i/m_{\text{e}})^{1/2}\sim 271$.

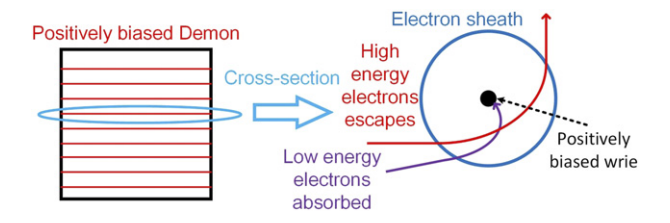


Figure 2. A simple diagram of an angular momentum trap.

loss flux contributed by low energy electrons are much higher for $d\Gamma_{electrode}$ than for $d\Gamma_{wall}$ due to the lack of an energy selective ion sheath.

In the same time, the additional loss of electrons also raises the plasma potential of the wall to reduce total electron loss, which improves the confinement of hotter electrons. The changes of V_p can be calculated via electron—ion loss balance [4, 7] and the results were shown in figure 1(d). The increase in V_p shifts and reduces the energy differential loss flux of the wall on the higher energy side, as shown in figure 1(b), thus allowing higher energy electrons to be confined. Therefore, when one heats a plasma via electron absorption, one is expected to see both a reduction of cold electrons and an

increase of hotter ones. Ideally, sheath expansion is neglected and any 'small' electrode with a positive bias a few $T_{\rm e}/e$ above the plasma potential becomes an energy unselective loss area and $V_{\rm p}$ is raised according to figure 1(d). Practically sheath expansion causes an electrode to change its effective area, thus $V_{\rm p}$ does depend on the positive bias on the electrode.

It is important to note that the predictions shown in figure 1 does not immediately translates into the changes in EEDFs because EEDF formation involves electron production, thermalization, electron heating and loss. Any electron absorption technique only control electron loss and one must resolve production, heating and any energy transfer from energetic electrons to cold electrons (thermalization) along with electron loss, which would be highly device dependent and well beyond the scope of this work.

2.2. Energy selectivity of the angular momentum trap

The argument for an angular momentum (AMT) selection of electron absorption essentially is the following: when an electron approaches a cylindrical wire, if the velocity of the electron is lower than the local electric field of the electron

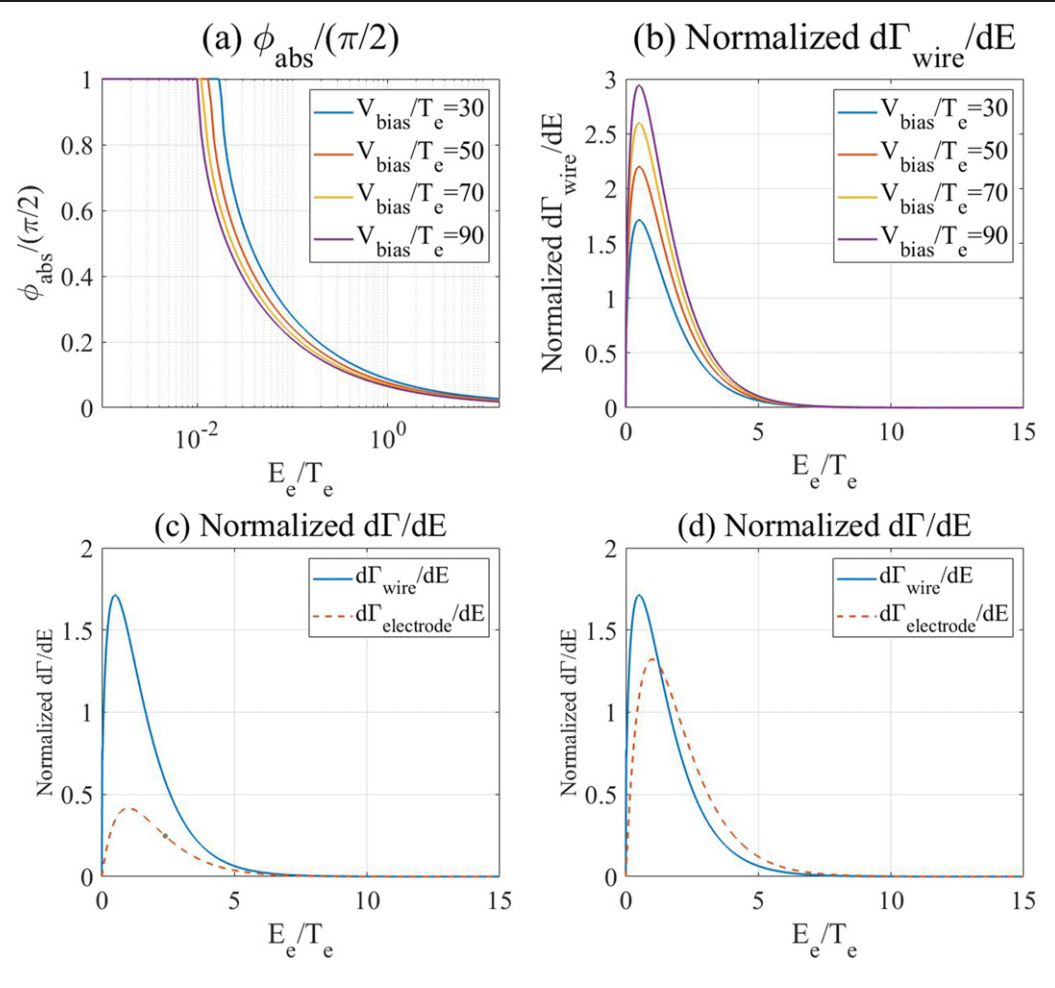


Figure 3. (a) Estimated absorption angle φ_{abs} vs temperature normalized electron energy E_e/T_e at various wire bias. (b) Estimated mechanical area normalized loss flux $(d\Gamma_{wire}/dE)/(v_{e,th}n_er_wL_{wire})$ vs E_e/T_e at various wire bias. (c) $(d\Gamma_{wire}/dE)$ of the angular momentum trap compared to $(d\Gamma_{electrode}/dE)$ with a solid electrode of equal geometrical surface area $(A_{electrode}/2\pi r_wL_{wire}=1)$. (d) $(d\Gamma_{wire}/dE)$ of the angular momentum trap compared to $(d\Gamma_{electrode}/dE)$ with a solid electrode of equal total electron absorption flux, $\Gamma_{wire}=\Gamma_{electrode}/2\pi r_wL_{wire}=3.18$).

sheath near a cylindrical wire, the electron becomes trapped by the electric field and is eventually absorbed into the wire, much like a version of the orbital motion limited theory for electrons. Figure 2 shows a simple diagram illustrating this effect. There has been numerous works on orbital motion limited theories [16–18], but for the experimental purpose of this work we analysis the effect of an electron angular momentum trap using a theory modified from Mott-Smith and Langmuir's simple and elegant model of ion orbital motion limited effects [19]. Consider an electron approaching the sheath boundary of a cylindrical collector with radius $r_{\rm w} = \lambda_{\rm Debye}/10$, where $\lambda_{\rm Debye}$ is the bulk plasma Debye length, biased at a positive voltage $V_{\rm bias}$ relative to $V_{\rm p}$, which forms a cylindrical sheath consist of a cylinder with radius $s_{\rm w}$ concentric to the wire. Note that $r_{\rm w}$ is chosen as $\lambda_{\text{Debye}}/10$ in order to ensure a cylindrical sheath instead of a planar sheath near the wire. The electron velocity relative to the wire at the sheath boundary can be decomposed in the radial component u and tangential component v. Consider also the electron's velocity components at the wire's radius u_r and v_r . Energy and angular momentum conservation states that

$$\frac{1}{2}m_{\rm e}(u_{\rm r}^2+v_{\rm r}^2) = \frac{1}{2}m_{\rm e}(u^2+v^2) + eV_{\rm bias},\tag{3}$$

$$r_{\mathbf{w}}v_{\mathbf{r}} = s_{\mathbf{w}}v. \tag{4}$$

And we can solve for u_r to obtain [19]

$$u_{\rm r}^2 = u^2 - \left(\frac{s_{\rm w}^2}{r_{\rm w}^2} - 1\right)v^2 + 2\frac{eV_{\rm bias}}{m_{\rm e}}.$$
 (5)

Here we can make a similar assertion of Mott-Smith and Langmuir that only electrons with u > 0 and $u_r^2 > 0$ will be absorbed into the wire. In the same time, we note that the electron's kinetic energy $E_e = m_e(u^2 + v^2)/2$, and that the electron incident angle φ can be defined as

$$\tan(\varphi) = \frac{v}{u}.\tag{6}$$

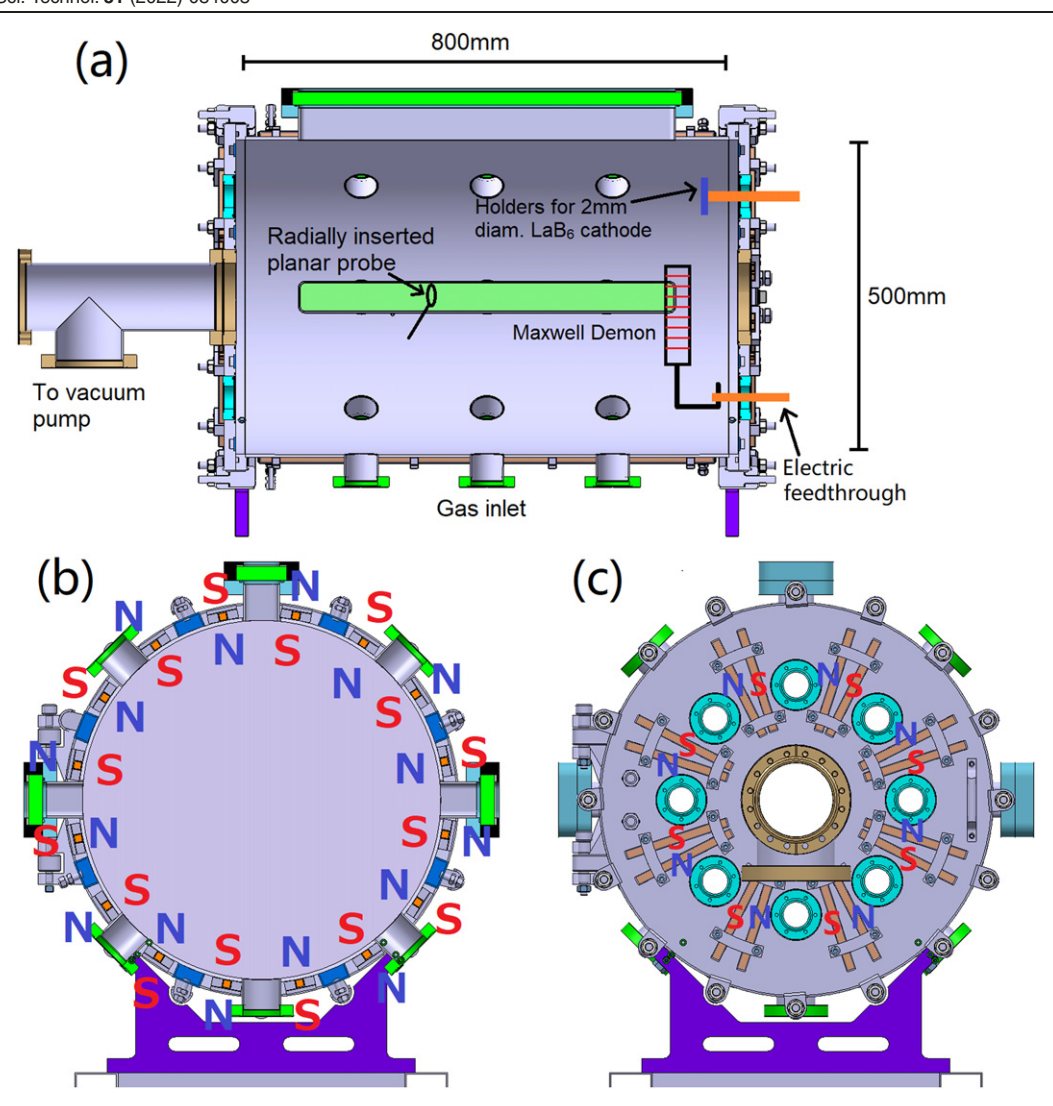


Figure 4. (a) An overall schematic of the DTS-II and its configuration in this study. (b) The configurations of the permanent magnets on the radial wall. (c) The configurations of the permanent magnets on the end walls.

Table 1. Parameters of the Maxwell demon and the different planar electrodes used as control experiments in this work.

Composition	Surface area (mm ²)	Area ratio to Maxwell demon
Maxwell demon (44 × 10 cm long, 0.025 mm diameter tungsten wires)	345 ± 10	1
15 mm diameter tantalum plate	353 ± 10	~ 1.02
26 mm diameter tantalum plate	1060 ± 30	~3.07
40 mm diameter tantalum plate	2512 ± 60	~7.28
150 mm diameter stainless steel plate	~35 300	~100

Writing equation (5) in terms of these definitions and solving for $u_r^2 > 0$ yields

$$\frac{E_{\rm e} + eV_{\rm bias}}{\frac{s_{\rm w}^2}{r_{\rm c}^2}E_{\rm e}} > \sin^2(\varphi). \tag{7}$$

Thus the critical incident angle $\varphi_{abs}(E_e)$ below which an electron is absorbed by the positively biased wire at each wire

bias can be calculated from equation (7). $\varphi_{abs}(E)$ is graphed against E in figure 3(a). Note that there is an electron energy limit $E_{\rm e}=eV_{\rm bias}/(s_{\rm w}^2/r_{\rm w}^2-1)$ below which $\sin^2(\varphi)>1$ and equation (7) becomes unsolvable. It is also noteworthy that at the limit $E_{\rm e}\gg eV_{\rm bias}$, $\sin(\varphi)=r_{\rm w}^2/s_{\rm w}^2$ which means the lack of angular momentum effects and electrons can only be lost by direct incidence to the wire surface. This is the critical value that all incident electrons are absorbed. Consider isotropic

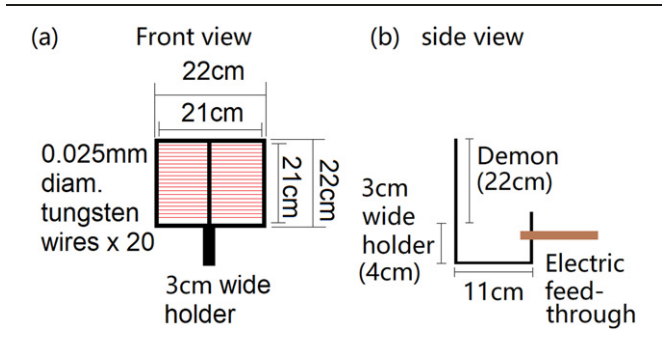


Figure 5. A simple schematic of the (a) front view and (b) side view of the Maxwell demon employed in this study.

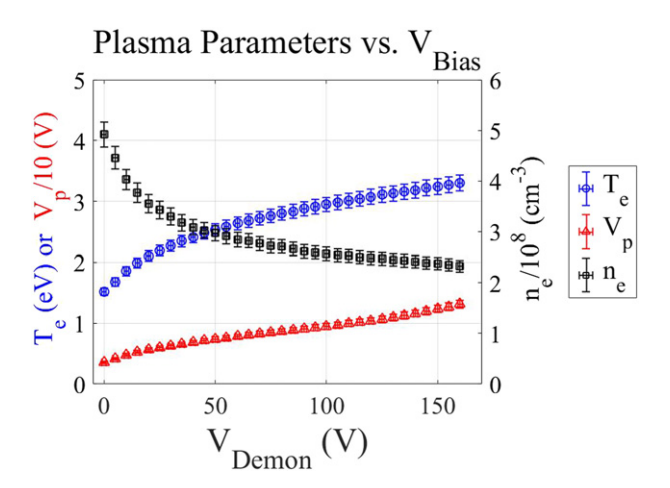


Figure 6. Evolution of the plasma parameters with the bias voltage on the Maxwell demon.

incidence onto the wire with incident angles from $-\pi/2$ to $\pi/2$, then the loss flux of the electrons onto the wire can be estimated as

$$d\Gamma_{\text{wire}}(E_{\text{e}}) = v_{\text{e}}(E_{\text{e}}) f_{\text{e}}(E_{\text{e}}) n_{\text{e}} \left(2\pi L_{\text{w}} s_{\text{w}}(V_{\text{bias}}) \right.$$

$$\times \frac{\varphi_{\text{abs}}(E_{\text{e}}, V_{\text{bias}})}{\frac{\pi}{2}} \right) dE_{\text{e}}, \tag{8}$$

where $L_{\rm w}$ is the wire length of the angular momentum trap. A normalized $d\Gamma_{\text{wire}}/(v_{\text{e,th}}n_{\text{e}}2\pi r_{\text{w}}L_{\text{wire}}) = (v_{\text{e}}(E_{\text{e}})/v_{\text{e,th}})$ $T_{\rm e}f_{\rm e}(E_{\rm e}/T_{\rm e})(s_{\rm w}(V_{\rm bias})/r_{\rm w}(2\varphi_{\rm bas}/\pi)){\rm d}(E_{\rm e}/T_{\rm e})$ can be defined as with the one associated with the energy unselective electrode. Figure 3(b) graphed $(d\Gamma_{wire}/dE)/(v_{e,th}n_e 2\pi r_w L_{wire})$ vs E_e/T_e calculated from equation (8) with various bias on the wire. This provides a sense of how the EEDF can be modified by the angular momentum trap. There are two distinctive features of $(d\Gamma_{wire}/dE)$ compared to the theoretical $(d\Gamma_{electrode}/dE)$. First, even normalized by its own geometrical area, $\Gamma_{\text{wire}} =$ $\int (d\Gamma_{\text{wire}}/dE)dE$ remains observably dependent on V_{bias} , this is clearly shown in figure 3(b) as the area under the normalized $d\Gamma_{\text{wire}}$ curves increase observably with V_{bias} . This is because the effective absorption area of the angular momentum trap is defined by the surface area of its cylindrical sheath $2\pi L_{\rm w} s_{\rm w}$, as opposed to the solid electrode which is expected to be limited by its geometrical area. Therefore, integrating the respective $d\Gamma$ over all electron energies, an angular momentum trap with $V_{\rm bias}/T_{\rm e}=30$, for example, absorbs as many electrons as a solid electrode with approximately 3 times its geometrical surface area, as shown in a comparison in figures 3(c) and (d). In addition, even with the same total electron loss flux $\Gamma_{\rm wire}=\Gamma_{\rm electrode}$, the angular momentum trap is shown to have significantly higher d $\Gamma_{\rm wire}$ at lower electron energy and a lower d $\Gamma_{\rm wire}$ at higher electron energy. This provides a quantitative comparison of energy selectivity between the angular momentum trap and the solid electrode and illustrates how the angular momentum trap can be more effective in electron heating.

Although $d\Gamma_{wire}$ and $d\Gamma_{electrode}$ do not immediately translate into changes in EEDFs as plasma heating and productions must be resolved to account for EEDF production, these calculations explains how Mackenzie's Maxwell demons have been observed to heat a plasma via electron absorption as effective as a solid electrode a few times its surface area [3].

It is also noteworthy that both the calculations of $d\Gamma_{\text{wire}}$ and $d\Gamma_{electrode}$ assumes electrons enter the electron sheaths near these devices with a random thermal flux. However, a recent theory suggests the presence of an electron presheath that accelerates electrons into a flowing electron Bohm speed $\sim (kT_{\rm e}/m_{\rm e})^{1/2}$ into the electron sheath [20–22]. The presence of an electron presheath or otherwise the electron Bohm criterion will change the energy selectivity of the demon as they changed the EEDF near the demon, causing low energy electrons to become $\sim T_e/2$ more energetic and cause some of the electrons originally moving away from the demon to approach the demon as slow electrons and be absorbed. Electron acceleration by the electron presheath also reduces the electron incident angle φ , which results in anisotropic electron incidence and facilitates stronger electron absorption. Since the electron energy gain associated with an electron presheath is on the order of $kT_e/2$, the presence of an electron presheath is expected to affect the absorption of low energy electrons $(E_{\rm e} < kT_{\rm e})$ more than higher energy ones. The electron presheath also introduce a density drop along that presheath due to flux conservation, which reduce the flux of both low energy and high energy electrons. These effects might mitigate each other and to resolve all of them would require a far more complicated computational model which unfortunately would be out of the scope of this work.

3. Experimental setup

Experiments were performed in the diagnostic test source-II (DTS-II) at the Institute of Plasma Physics, within the Chinese Academy of Sciences. A schematic of the device is shown in figure 4. The cylindrical chamber is 500 mm in diameter and 800 mm long. The plasma discharge was created by thermionically emitted electrons accelerated to the chamber wall to produce ionization of the feedstock gas, argon in our case. Thermionically emitted electrons, or primary electrons, were confined using rows of neodymium magnets fastened to the chamber walls. On both end wall flanges and the radial wall, 16 rows of magnets, each row of uniform polarity, were fastened to the chamber with rows alternating in polarity, to produce a surface magnetic multi-dipole confinement. The polarities of the radial and end wall permanent magnets are

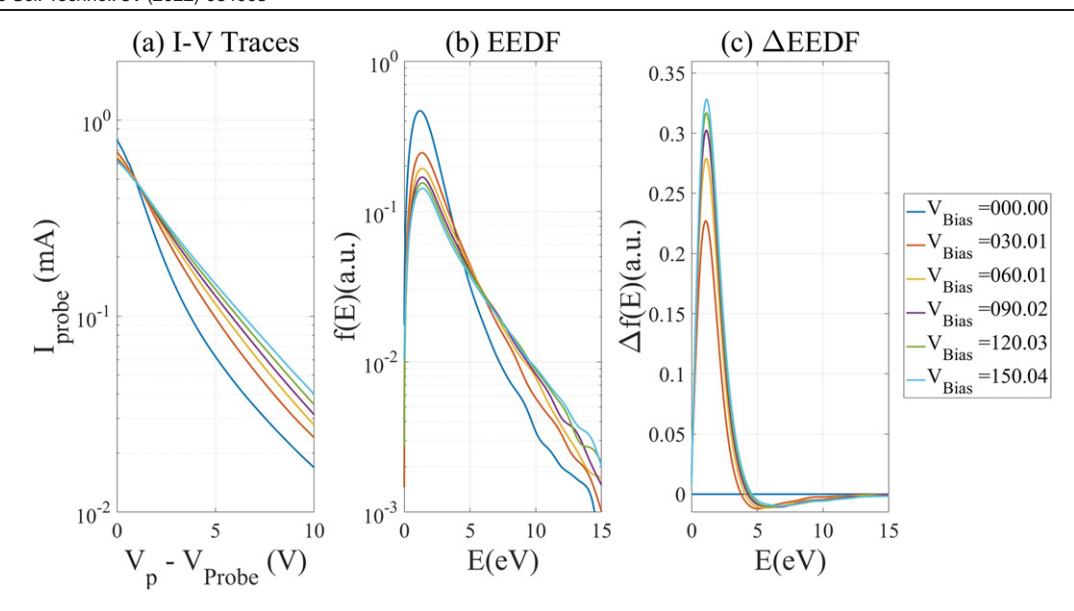


Figure 7. (a) I-V traces of the Langmuir probe, (b) the corresponding EEDFs extracted from these traces, (c) changes of the EEDFs (Δ EEDF) $\Delta f(E) = f_0(E) - f(E)$ with various bias on the Maxwell demon.

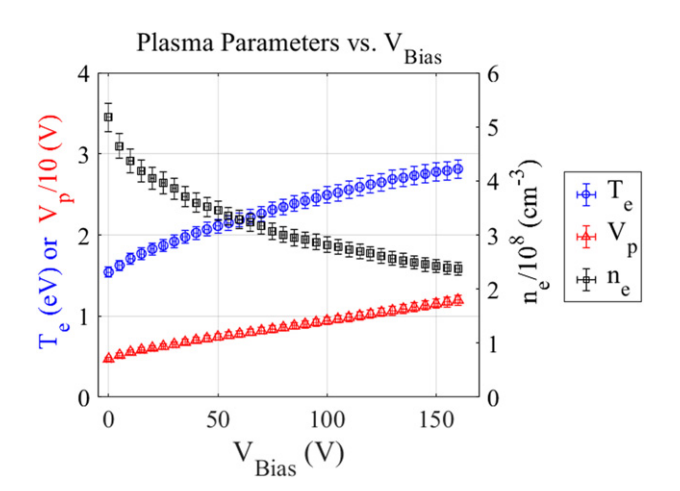


Figure 8. Evolution of the plasma parameters with the bias voltage on the 15 mm planar electrode.

illustrated in figures 4(b) and (c). The multi-dipole configuration leaves a magnetic field at the center of the chamber less than 1 G, leaving the bulk plasma unmagnetized. Primary electrons were produced by direct current heating of a 2 mm diameter, 15 cm long LaB₆ rod cathode. The multi-dipole confined DC hot cathode discharge produces an unmagnetized and quiescent plasma.

Experiments were performed with argon gas at a neutral pressure $P_{\rm Ar}=0.015\pm0.002$ Pa, a cathode bias $V_{\rm prim}=-140$ V, and a discharge current of 0.05 A, this results in a plasma density $n_{\rm e0}=5.2\pm0.4\times10^8$ cm⁻³, an electron temperature $T_{\rm e0}=1.5\pm0.1$ eV, and a plasma potential $V_{\rm p0}=4.5\pm1$ V without the use of the Maxwell demon and a positively biased electrode. This set of parameters are chosen to obtain a large Debye length $\lambda_{\rm Debye}=0.4\pm0.03$ mm, much larger than the 0.025 mm diameter tungsten wires that compose the Maxwell demon. A large Debye length maximizes orbital motion limitation effects and thus maximizes the

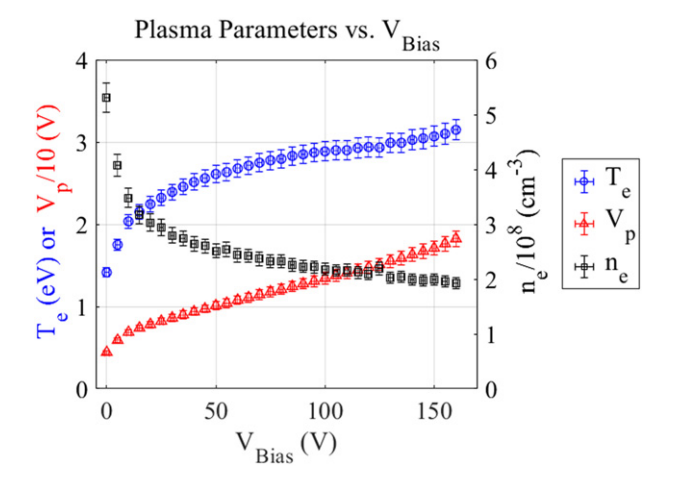


Figure 9. Evolution of the plasma parameters with the bias voltage on the 26 mm planar electrode.

demon's expected effect as an angular momentum trap. The Mackenzie's Maxwell demon is employed near one end of the device being installed from a radial window. In addition to this, a set of tantalum and stainless steel plates at various diameters are used to replace the demon as a control experiment for comparison between a demon and a pure adjustment of loss area. The dimensions of these planar electrodes are described in table 1. A 6 mm diameter, tantalum planar Langmuir probe and is inserted into the bulk plasma approximately in the chamber's center through one of the radial windows to measure the axial EEDF and the plasma potential $V_{\rm p}$.

Here we adopted an improved automated I-V trace analysis technique from reference [23, 24] which automatically fits the multi-Maxwellian EEDFs and uses the effective temperature and plasma density as the iterative fitting parameters for the power-law depending ion saturation current. To avoid a bias toward the cold electron population to obtain a more consistent result particularly in situations where the cold electron population becomes very small and is difficult to be determined,

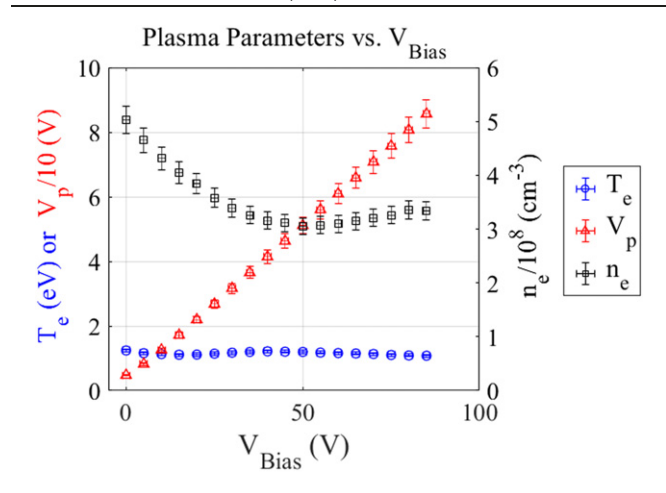


Figure 10. Evolution of the plasma parameters with the bias voltage on the 150 mm planar electrode.

the arithmetic mean $\int Ef(E) dE$ of the EEDF is adopted as the effective electron temperature $T_{\rm eff}$. This results in an agreement of fitting single Maxwellian, bi-Maxwellian and triple Maxwellian $T_{\rm eff}$'s within 5%–10%, well within the typical Langmuir probe measurement errors. EEDFs are also calculated from the I-V traces via the Druyvesteyn method, i.e. taking the second derivative of the I-V trace [25, 26].

A schematic of the design of the Mackenzie's Maxwell demon employed in this experiment as a test for the angular momentum trap is shown in figure 5(a). As shown in the figure, a 1 mm thick stainless steel sheet is laser cut into a metal frame with two $\sim 10 \text{ cm} \times 20 \text{ cm}$ inner rectangular spaces to accommodate 2×22 equally spaced 0.025 mm tungsten wires. The rectangular frame is 0.5 cm wide and is supported by a 3 cm wide holder which is affixed to an electric feedthrough from an end wall with the demon itself extended into the bulk plasma, as shown in figure 5(b). The frame of the demon is covered by a ceramic coating, and the vacuum feedthrough along with its interface with the demon's holder is covered by fiberglass. This ensures that only the thin tungsten wires are electrically exposed to the plasma. The 20 cm long space makes this version of the demon approximately equal to the 80 wires demon used in previous studies [2, 3], and the \sim 9 mm separation between the wires better ensures an adequate distancing between wires to minimize sheath overlapping so that each wire serves as an angular momentum trap if such effect indeed exist.

4. Experimental results

Evolution of the plasma parameters with the bias voltage on the Maxwell demon is shown in figure 6. The I-V traces, the corresponding EEDFs and the changes of the EEDFs (Δ EEDF) $\Delta f(E) = f(E) - f_0(E)$ with respect to the EEDF without the influence of the demon $f_0(E)$ are graphed in figure 7.

As shown in the figures, increasing the demon bias voltage increases T_e along with V_p , and the evolution of the I-V traces shows that the demon reduced a bi-Maxwellian EEDF to a single Maxwellian one, consistent with previous studies [2, 3]. The evolution of the EEDF shows both reduction of low energy

electrons and increase of high energy ones, clearly illustrated by the \triangle EEDFs in figure 7(c). This result is consistent with the loss flux predictions illustrated in section 2. From equation (8) and the change of the loss flux $d\Gamma_{\text{wire}}$ graphed in figure 3(b), the loss of low energy electrons is elevated due to the energy selective loss Maxwell demon, therefore raising the electron temperature of the bulk plasma. On the other hand, any additional loss of electrons or increase of $T_{\rm e}$ raises $V_{\rm p}$ due to changes in electron-ion loss balance [4, 7]. Increase in V_p causes higher energy electrons to be better confined. This effect is illustrated with equation (1) and graphed in figure 1(b), as the loss of higher energy electrons decreases with increasing V_p . In addition, due to the energy selectivity of the Maxwell demon, these additionally retained hot electrons are not re-absorbed into the demon and therefore they can stay in the plasma. This results in both the observably higher amount of hot electrons as shown in figure 7, and a minimal disturbance of V_p and n_e as the demon heats the plasma electrons. The latter effect is discussed later in this section.

For comparison, figures 8-10 show the evolution of the plasma parameters affected by the bias voltage on the 15 mm diameter plate, the 26 mm diameter plate, and the 150 mm diameter plate respectively, and figures 11-13 shows the I-Vtraces, the EEDFs, and the Δ EEDFs under the influence of bias voltage on these electrodes respectively. As shown in the figures, these electrodes are also capable of heating the electrons simply by indiscriminative absorption, although the demon performance is very similar to that of the 26 mm diameter planar electrode in both the $T_{\rm e}$ vs $V_{\rm bias}$ characteristic and the changes in the EEDF as $T_{\rm e}$ is raised, which has a much larger surface area than the demon, in terms of bias voltage vs electron temperature characteristics. This is consistent with previous experiments [3] and might be accounted by the fact that the effective area of the demon has been greatly expanded by the cylindrical sheath around the thin tungsten wires, which is consistent with the predictions shown in figure 3(b). However, the increase of hot electrons as $T_{\rm e}$ is raised by the planar electrodes is smaller than that when $T_{\rm e}$ is being raised by the demon. This is shown in the $\Delta EEDFs$ with the exception of the 26 mm diameter plate and only when the bias is relatively low $(V_{\rm bias} < 60)$. This indicates that although plasma potential does increase with $T_{\rm e}$ in these devices, the elevated confinement of hot electrons was offset by their indiscriminative loss to the electrode. This effect will be discussed in detail later in this manuscript. These results are consistent with the comparison shown in figure 3(c).

In an extreme case for these studies, the bias voltage on the 150 mm diameter electrode increases only the plasma potential with little to no electron heating at all. These results were in sharp contrast with previous experiments which showed that a large electrode does heat the plasma as well as increase $V_{\rm p}$ [2, 3, 5, 7]. However, our results are consistent with Mackenzie's original work [1]. The most pronounced differences in experimental setup between this work and the previous ones are the installation of multi-dipole confinement magnets that better encircled the plasma volume with the presence of the end-wall magnets, and the absence of other submerged planar electrodes in this work. Having benefited

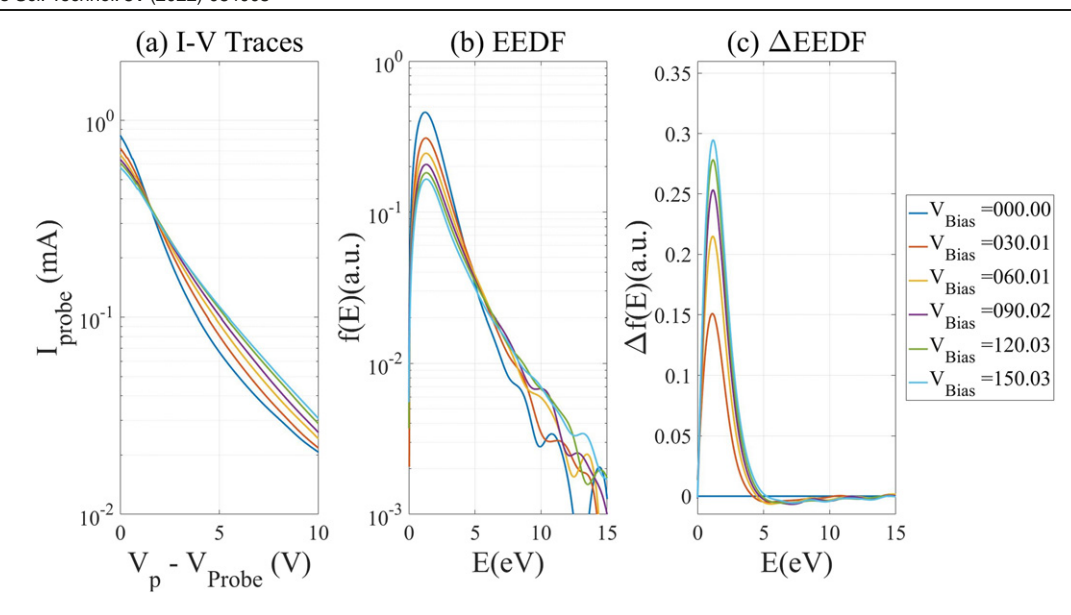


Figure 11. (a) I-V traces of the Langmuir probe, (b) the corresponding EEDFs extracted from these traces, (c) changes of the EEDFs (Δ EEDF) $\Delta f(E) = f_0(E) - f(E)$ with various bias on the 15 mm diameter planar electrode.

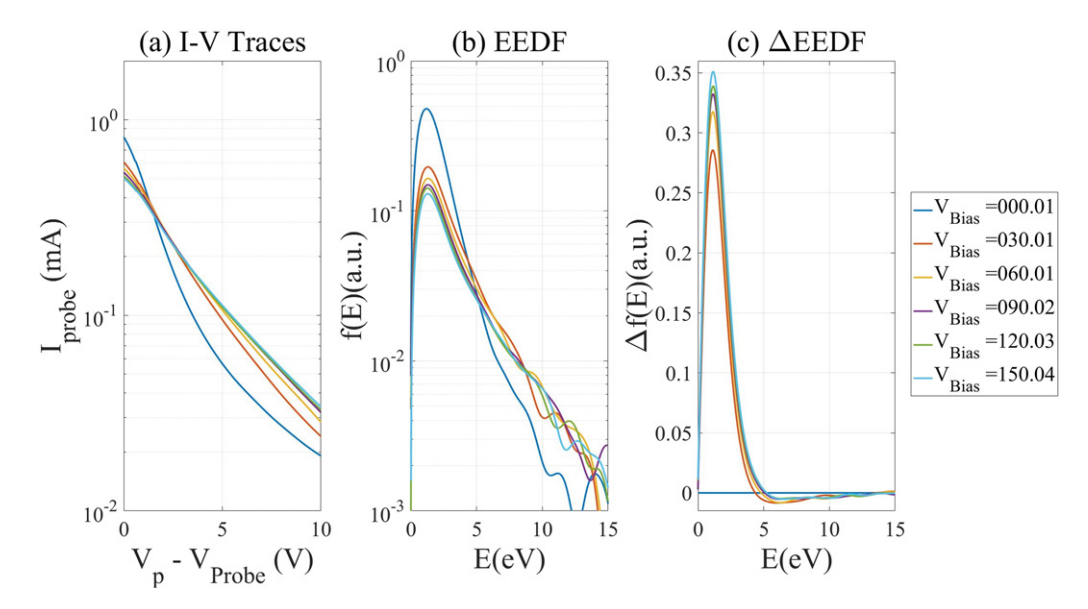


Figure 12. (a) I-V traces of the Langmuir probe, (b) the corresponding EEDFs extracted from these traces, (c) changes of the EEDFs (Δ EEDF) $\Delta f(E) = f_0(E) - f(E)$ with various bias on the 26 mm diameter planar electrode.

from a newly designed fixture from the end walls, both the demon and the electrodes in this experiment are more thoroughly immersed into the bulk plasma, being placed across the axial center of the device, where in some of the previous studies [2, 3] they are placed near the chamber's radial walls. This causes all electrodes to avoid the radial multi-dipole confinement fields and avoided their associated edge effects. Both differences could contribute to the different results. On the other hand, the fact that $V_{\rm p}$ is consistently only $\sim\!0.5T_{\rm e}$ above the electrode bias is expected to be a cooling effect rather than heating effect as all electrons at higher energies are lost to a very large area surface. In any event, the results do strongly indicate that electron energy selectivity remains a very strong factor of how a loss area modifies plasma EEDFs.

One way energy selectivity affects heating performance is the density reduction concomitant with electron heating. Relatively better energy selectivity implies a smaller reduction in electron density for a given increase in electron temperature, as fewer hot electrons are removed. Figure 14 shows the plasma density relative to the density found with a grounded demon or plate electrode, $n_{\rm e}/n_{\rm e0}$, graphed against the increase in electron temperature $\Delta T_{\rm e} = T_{\rm e} - T_{\rm e0}$ under the influence of these different heating methods. As shown in the figure, all the solid electrodes essentially result in the same density reduction per temperature increase. This reflects absence of the voltage bias on the electrode in equation (2), and that only the absorption area of the electrode affects the electron loss flux into the electrode. It remains possible to raise $T_{\rm e}$ with

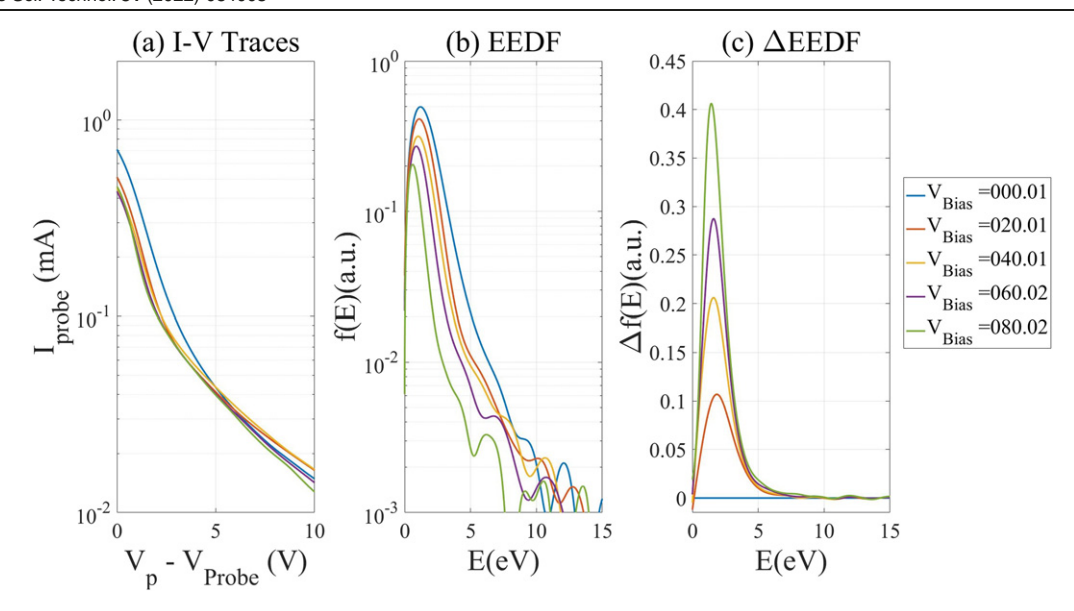


Figure 13. (a) I-V traces of the Langmuir probe, (b) the corresponding EEDFs extracted from these traces, (c) changes of the EEDFs (Δ EEDF) $\Delta f(E) = f_0(E) - f(E)$ with various bias on the 150 mm diameter planar electrode.

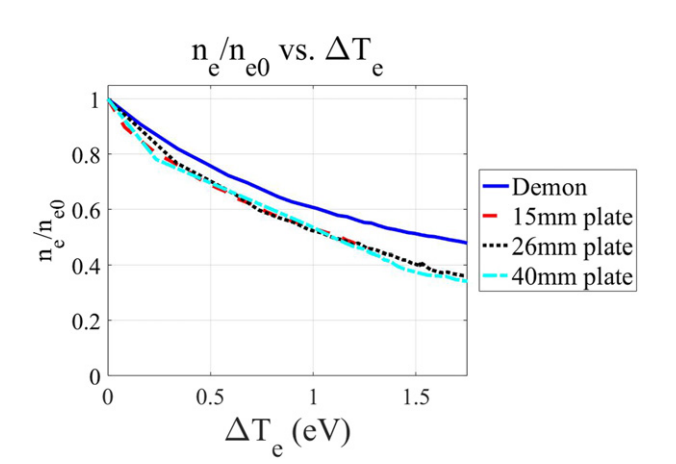


Figure 14. Proportional plasma density $n_{\rm e}/n_{\rm e0}$ graphed against the raise in electron temperature $\Delta T_{\rm e}=T_{\rm e}-T_{\rm e0}$ under the influences of different heating methods.

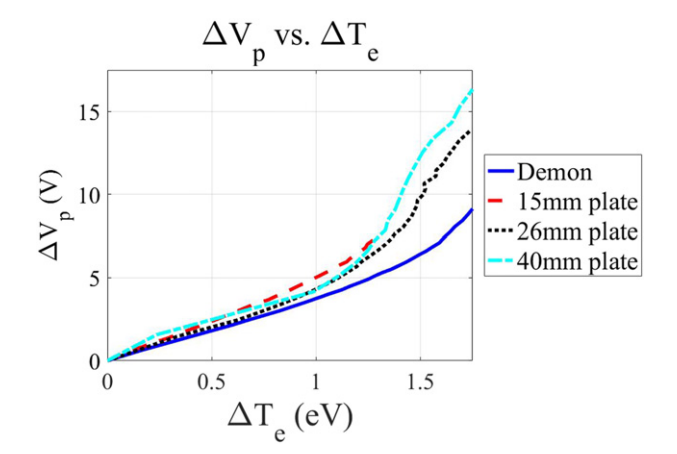


Figure 15. Raise in plasma potential $\Delta V_{\rm p}=V_{\rm p}-V_{\rm p0}$ graphed against the raise in electron temperature $\Delta T_{\rm e}=T_{\rm e}-T_{\rm e0}$ under the influences of different heating methods.

increasing bias on the electrodes because the effective area of the electrodes increases with the positive bias applied on them. This makes an increasing bias on a solid electrode effectively the same as replacing the electrode with a bigger one. Thus, the $T_{\rm e}$ vs $n_{\rm e}/n_{\rm e0}$ evolution of all solid plates remains on the same curve regardless of their geometrical size. On the other hand, the Maxwell demon follows another curve with a smaller proportional electron density drop compared to the planar electrodes, this is because the Maxwell demon is energy selective and absorbs more absorption of the low energy electrons than the solid electrodes, as shown in figure 3(c), thus requires less density drop for the same temperature raise.

Another illustration of how energy selectivity of electron heating techniques affects plasma parameter formation is to look at how the plasma potential changes with the electron temperature under the influences of different heating methods. This is illustrated in figure 15. Note that the formation of the plasma potential is essentially a matter of electron—ion loss

balance, which is determined by total electron loss and total ion loss from a plasma [5-7]. Conversely, one can reduce the plasma potential by injecting electrons into a plasma from an external source [2]. Thus a better energy selective loss area, removing less hot electrons, is also expected to result in smaller increase in V_p per T_e increase. This effect is particularly observable at higher $\Delta T_{\rm e}$ where the higher bias voltage on the 40 mm and 26 mm plate expands their effective areas to close to the $A_{\text{electrode}} = 2.3 A_{\text{wall}} (m_{\text{e}}/m_{\text{i}})^{1/2}$ limit, and thus more abruptly increase V_p , as illustrated in figure 1(d). This reflects that the change of electron loss with these electrodes follows the conventional theory on electron-ion loss balance where the electrode serves only as an additional electron loss area [4, 7]. The $\Delta V_{\rm p}$ vs $\Delta T_{\rm e}$ under the effects of the Maxwell demon, on the other hand, follows a smaller ΔV_p evolution, particularly at higher $\Delta T_{\rm e}$. This deviation reflects the fact that not all electrons enters the demon's electron sheath is absorbed, as higher energy electrons are likely to escape via orbital motion, as prediction from equation (8).

5. Conclusion

The comparison of MacKenzie's Maxwell demon and a series of planar electrodes has been revisited to investigate whether the Maxwell demon indeed is more energy selective than a planar electrode simply absorbing electrons indiscriminately, and whether such selectivity has consequences on the devices' tailoring of the plasma parameters. In this process, we have attempted to quantify the effects of energy selectivity looking both directly at the evolution of the plasma EEDF and the resultant changes in the overall plasma parameters.

The results show clear distinctions between devices of different supposed energy selectivity, with increasing energy selectivity devices providing better absorption of sufficiently low energy electrons. These results agree well with theoretical comparison of the heating performance of the two electron absorption heating methods associated with their heating mechanisms. Current evidence remain supportive of MacKenzie's claim that the Maxwell demon heats the electrons via angular momentum trap effects, which manifests in its higher selectivity to absorb low energy electrons as demonstrated by the changes of the EEDFs at various bias applied to the difference devices of electron heating. This also caused the experimental observation of the higher heating efficiency per plasma density reduction and higher heating efficiency per plasma potential elevated by the demon compared to planar electrode, particularly when using these devices at the limit of their performances, i.e. at very high voltage bias. With orbital limited motion effects, particularly for ions, being a very well-known issue, it might not be surprising that electrons can also exhibit similar effects to a grid of very thin, positively biased wires.

Acknowledgments

This work is supported by National Natural Science Foundation of China (contract No. 11875285), National Research Foundation of Korea funded by Ministry of Science and ICT (Grant Nos. NRF-2020M1A7A1A03016161 and NRF-2021R1A2C2005654), and the US National Science Foundation (NSF PHY-1804240 and NSF PHY-2108636).

Data availability statement

All data that support the findings of this study are included within the article (and any supplementary files).

ORCID iDs

Chi-Shung Yip https://orcid.org/0000-0003-4475-8000
Chenyao Jin https://orcid.org/0000-0002-4289-3578
Wei Zhang https://orcid.org/0000-0002-9854-8028
Di Jiang https://orcid.org/0000-0002-6370-2611
Young-Chul Ghim https://orcid.org/0000-0003-4123-9416
Greg Severn https://orcid.org/0000-0002-4794-5170

References

- [1] MacKenzie K R, Taylor R J, Cohn D, Ault E and Ikezi H 1971 Appl. Phys. Lett. 18 529
- [2] Yip C-S and Hershkowitz N 2015 Plasma Sources Sci. Technol. 24 034004
- [3] Yip C-S, Sheehan J P, Hershkowitz N and Severn G 2013 Plasma Sources Sci. Technol. 22 065002
- [4] Baalrud S D, Scheiner B, Yee B T, Hopkins M M and Barnat E 2020 Plasma Sources Sci. Technol. 29 053001
- [5] Barnat E V, Laity G R and Baalrud S D 2014 Phys. Plasmas 21 103512
- [6] Baalrud S D, Longmier B and Hershkowitz N 2009 Plasma Sources Sci. Technol. 18 035002
- [7] Baalrud S D, Hershkowitz N and Longmier B 2007 Phys. Plasmas 14 042109
- [8] Arslanbekov R R and Kudryavtsev A A 1998 Phys. Rev. E 58 6539–52
- [9] Kortshagen U, Parker G J and Lawler J E 1996 Phys. Rev. E 54 6746–61
- [10] Kaganovich I, Mišina M, Berezhnoi S V and Gijbels R 2000 Phys. Rev. E 61 1875–89
- [11] Scheiner B, Baalrud S D, Hopkins M M, Yee B T and Barnat E V 2016 Phys. Plasmas 23 083510
- [12] Hershkowitz N 2005 Phys. Plasmas 12 055502
- [13] Stenzel R L, Gruenwald J, Ionita C and Schrittwieser R 2012 Plasma Sources Sci. Technol. 21 015012
- [14] Song B, D'Angelo N and Merlino R L 1991 J. Phys. D: Appl. Phys. 24 1789
- [15] Scheiner B, Beving L and Baalrud S D 2019 Phys. Plasmas 26 013509
- [16] Bernstein I B and Rabinowitz I N 1959 Phys. Fluids 2 112-21
- [17] Lampe M 2001 J. Plasma Phys. 65 171–80
- [18] Laframboise J G and Parker L W 1973 Phys. Fluids 16 629–36
- [19] Mott-Smith H M and Langmuir I 1926 Phys. Rev. 28 727–63
- [20] Hood R, Baalrud S D, Merlino R L and Skiff F 2020 Phys. Plasmas 27 053509
- [21] Yee B T, Scheiner B, Baalrud S D, Barnat E V and Hopkins M M 2017 Plasma Sources Sci. Technol. 26 025009
- [22] Scheiner B, Baalrud S D, Yee B T, Hopkins M M and Barnat E V 2015 Phys. Plasmas 22 123520
- [23] Yip C-S, Zhang W, Xu G and Hershkowitz N 2020 Plasma Sci. Technol. 22 085404
- [24] Lim Y et al 2022 Plasma Sources Sci. Technol. 31 024001
- [25] Godyak V A and Demidov V I 2011 J. Phys. D: Appl. Phys. 44 233001
- [26] Druyvesteyn M J and Penning F M 1940 Rev. Mod. Phys. 12 87–174